View metadata, citation and similar papers at core.ac.uk

brought to you by CORE

provided by Institutionelles Repositorium der Leibniz Universität Hannover

New design of electrostatic mirror actuators for application in high-precision interferometry

This content has been downloaded from IOPscience. Please scroll down to see the full text.

2015 Class. Quantum Grav. 32 175021

(http://iopscience.iop.org/0264-9381/32/17/175021)

View the table of contents for this issue, or go to the journal homepage for more

Download details:

IP Address: 194.95.157.141
This content was downloaded on 03/08/2016 at 09:22

Please note that terms and conditions apply.

OPEN ACCESS
IOP Publishing
Classical and Quantum Gravity
Class. Quantum Grav. **32** (2015) 175021 (11pp)
doi:10.1088/0264-9381/32/17/175021

New design of electrostatic mirror actuators for application in high-precision interferometry

H Wittel[1], S Hild[2], G Bergmann[1], K Danzmann[1] and K A Strain[1,2]

[1] Max-Planck-Institute for Gravitational Physics and Leibniz Universität Hannover, D-30167 Hannover, Germany
[2] SUPA, School of Physics and Astronomy, The University of Glasgow, Glasgow, G12 8QQ, UK

E-mail: Holger.Wittel@aei.mpg.de

Received 17 November 2014, revised 1 July 2015
Accepted for publication 22 July 2015
Published 19 August 2015

Abstract

We describe a new geometry for electrostatic actuators to be used in sensitive laser interferometers, suited for prototype and table top experiments related to gravitational wave detection with mirrors of 100 g or less. The arrangement consists of two plates at the sides of the mirror (test mass), and therefore does not reduce its clear aperture as a conventional electrostatic drive (ESD) would do. Using the sample case of the AEI-10 m prototype interferometer, we investigate the actuation range and the influence of the relative misalignment of the ESD plates with respect to the test mass. We find that in the case of the AEI-10 m prototype interferometer, this new kind of ESD could provide a range of 0.28 μm when operated at a voltage of 1 kV. In addition, the geometry presented is shown to provide a reduction factor of about 100 in the magnitude of the actuator motion coupling to the test mass displacement. We show that therefore in the specific case of the AEI-10 m interferometer, it is possible to mount the ESD actuators directly on the optical table without spoiling the seismic isolation performance of the triple stage suspension of the main test masses.

Keywords: interferometry, actuator, electrostatic drive

Content from this work may be used under the terms of the Creative Commons Attribution 3.0 licence. Any further distribution of this work must maintain attribution to the author(s) and the title of the work, journal citation and DOI.

1. Motivation

Interferometric gravitational wave detectors, such as GEO 600 [1], advanced LIGO (aLIGO) [2], Advanced Virgo [3] and KAGRA [4] are large laser interferometers with the mirrors/test masses hung at the bottom of multi-stage pendulum chains. For the operation of these detectors, it is necessary to have low-noise, contact-free actuators for controlling the longitudinal and angular degrees of freedom of the mirrors. This is traditionally done with either magnet-coil actuators or electrostatic drives (ESDs). GEO 600 has operated since 2001 with ESDs as the main longitudinal actuators for controlling the differential arm length. Based on this experience, ESDs are now employed in aLIGO [5], using a very similar configuration to the original GEO 600 design. The GEO/aLIGO ESDs are designed in the form of a metallic comb structure that has been coated onto a reaction mass and is located a few millimeters behind the mirror. Schematic drawings and a photograph of this conventional ESD setup are shown in figure 1. The ESD on the reaction mass needs its own seismic isolation to avoid the coupling of ground motion to the seismically isolated test mass. Therefore, it is also hung as the lowest stage of a multi-stage pendulum, which again requires its own sensors and actuators for alignment and damping of the reaction mass. Further practical issues in hanging two multi-stage pendulums close to each other can arise. One particular issue that may introduce noise is squeezed film damping that arises due to residual gas in between the test- and reaction mass [6].

Furthermore, this conventional type of ESD reduces the possible free aperture in transmission. This may be problematic for experiments which require the largest possible free aperture, such as the planned AEI-10 m prototype interferometer [7, 8] or the speedmeter proof of principle experiment in Glasgow [9, 10].

With the AEI-10 m interferometer in mind, we investigate a new ESD configuration featuring a simpler geometry. This uses only two plates at the sides or at top and bottom of the mirror, as pictured in figure 3. Since the force that may be obtained per applied voltage of this setup is smaller than for the conventional ESD configuration, this type of ESD is mainly suited for the case of light ($\leqslant$100 g) mirrors such as in the AEI-10 m prototype interferometer or in the Glasgow speedmeter proof of principle experiment.

2. Basic principle

The working principle of ESDs is that an inhomogeneous electric field is built up in a dielectric medium (i.e. the mirror). If the mirror is not centered longitudinally between the plates, it will be subject to a force that pulls it towards the center of the plates. In order to analyze our new ESD design, we first turn to a simplified analytic model, before we use finite element (FE) simulations later. Our simplified model shall be the case of a dielectric slab inserted into a parallel-plate capacitor (as in [11]), which is pictured in figure 2. Calculating the force for this simple model is a standard problem in electrodynamics. The force is given by [11]:

$$F = (\epsilon_r - \epsilon_0) \cdot E_{\mathrm{D}} \cdot U_{\mathrm{ESD}}^2 / 2d_{\mathrm{plates}}, \tag{1}$$

where E_{D} is the plate depth, U_{ESD} is the voltage across the plates and d_{plates} is the plate separation. ϵ_0 and ϵ_r are dielectric constants (see also table 1 for the values and symbols used in this article). This formula is only valid under certain assumptions:

(i) There is no gap between the dielectric and the plates.
(ii) One end of the dielectric material is in a homogeneous electric field between the plates.

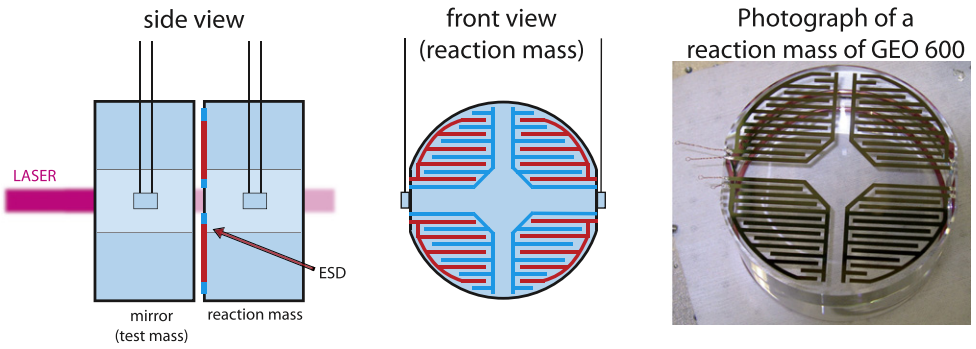

Figure 1. Left and center: schematic drawing of a conventional ESD setup. The ESD setup consists of four independent ESD comb-shaped electrode pairs on a single reaction mass. The anodes are colored in red, the cathodes are colored blue. The center of the reaction mass is kept free so that a laser beam can pass without significant clipping. Right: photograph of a reaction mass of GEO 600.

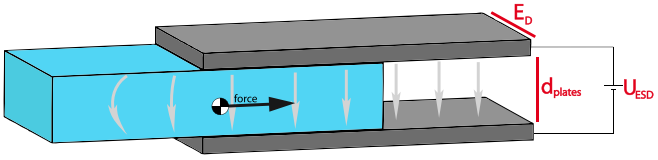

Figure 2. Illustration of the simple model. A slab of dielectric material between two parallel capacitor plates. The electric field is pictured as gray arrows.

Table 1. Properties used for the FE simulations presented in this document.

Mirror diameter	M_{D}	4.90 cm
Mirror thickness	M_{T}	2.45 cm
Mirror material	—	Fused silica
Mirror dielectric constant	ϵ_r	$3.7\epsilon_0$
Mirror mass	m	102 g
Pendulum length	l	20 cm
Lateral distance mirror-ESD	d_1	1.05 cm
Long. relative position mirror-ESD	d_2	3.075 cm
Applied voltage	U_{ESD}	1000 V
ESD dimensions (one plate)	$E_{\mathrm{W}} \times E_{\mathrm{H}} \times E_{\mathrm{D}}$	5 cm × 0.5 cm × 5 cm
ESD plate separation	d_{plates}	7 cm
Number of nodes	n_{nodes}	221 944

(iii) The other end of the dielectric is far outside of the plates; it does not 'see' the electric field of the plates.

We can use the formula for the simplified case to approximate the order of magnitude of the force that the ESD will provide. The exact strength of the force must be determined by FE methods, since none of the assumptions mentioned above is exactly fulfilled.

To estimate the force that the ESD can provide using the simplified formula, first we compute an effective dielectric constant $\epsilon_{r_{\mathrm{eff}}}$ for a mirror between the two plates, since it does not fill the space between the ESD plates completely. We determine a 'fill factor' of

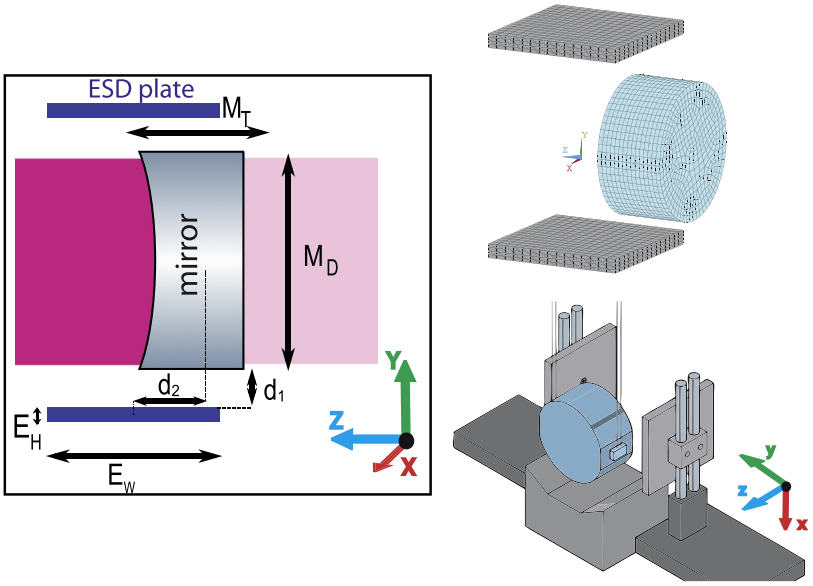

Figure 3. Left: basic geometrical setup of the ESD plates with respect to the main test masses/mirror. Please note that this sketch can be either side-view or top-view, depending on the actual installation. The probing laser beam is shown in purple while the beam transmitted through the mirror is painted with a lighter color. The dimensions M_T, M_D, E_H, E_W and $d_{1,2}$ are defined in table 1. Top right: view of the FE model that was used in this article. The elements modeling the space around mirror and ESD plates are omitted here for clarity. Bottom right: a mock up drawing of what a potential installation might look like.

$A_{\text{mirror}}/A_{\text{plates}} = \pi r_{\text{mirror}}^2/E_D \cdot d_{\text{plates}} = 0.54$. Now we can multiply the fill factor with ϵ_r and get an effective $\epsilon_{r_{\text{eff}}} = 2$. With the values given in table 1 and an $\epsilon_{r_{\text{eff}}} = 2$, equation (1) gives a position independent force of the order of some μN.

3. Quantitative analysis using FEM

The FEM simulations in this article were performed with the software ANSYS 13 [19], using the macro 'EMFT'. The parameters used throughout this analysis, unless noted otherwise, are given in table 1.

The origin of the coordinate system is located in the center between the ESD plates. The *Z*-axis points from the flat mirror surface to the center between the plates (sometimes called 'longitudinal direction' or 'beam direction'). The *Y*-axis points towards one of the plates and the *X*-axis is perpendicular to the *Y*- and *Z*-axes. Figure 3 shows the geometry of the new ESD setup. The force that the ESD applies on the mirror in dependence of the relative longitudinal position between mirror and ESD is plotted in figure 4. From this dependency we also find the best operating distance between mirror and ESD: the maximum and to first order flat force of 1.4 μN appears when the mirror is shifted by 3.075 cm relative to the ESD plates. We choose this position as our potential operating point. From the force, the magnitude of the ESD range can be deduced. We assume that the mirror is suspended as a pendulum of the length l. The full (dc) actuation range z_{dc} is reached when the pendulum back action force cancels the ESD-force:

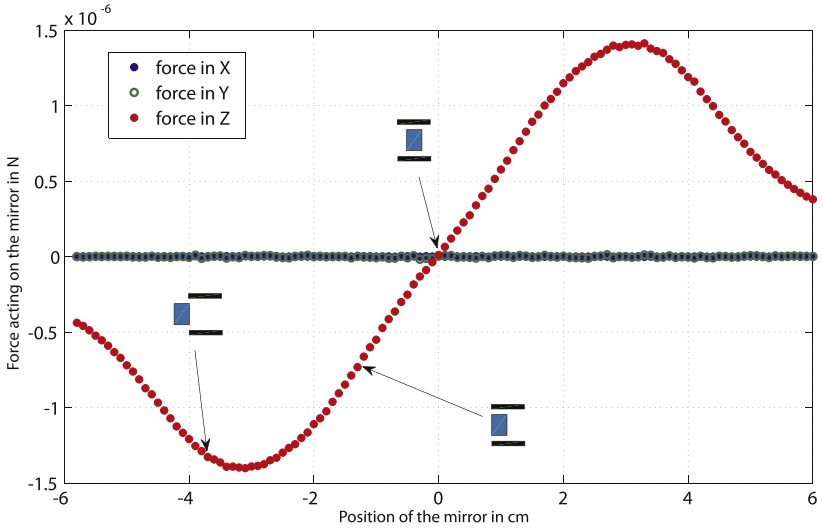

Figure 4. Longitudinal force on the mirror, versus relative longitudinal position of mirror and ESD. The x-axis shows the relative distance between the mirror center and the center of the capacitor plates.

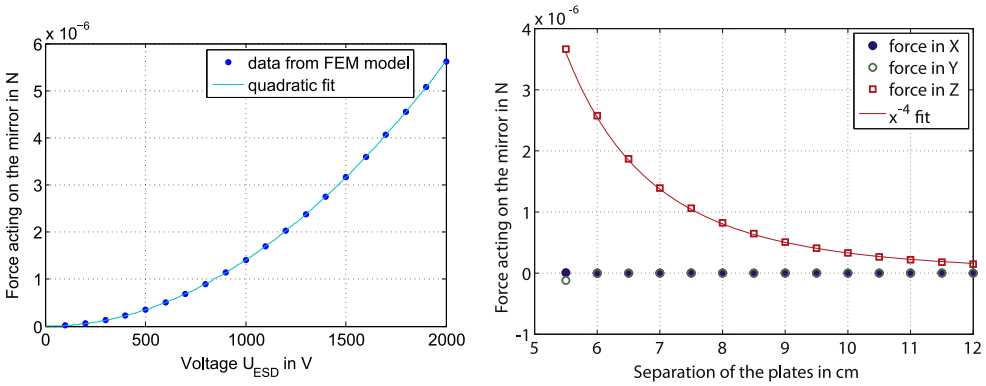

(a) Voltage change (b) Plate separation

Figure 5. Figure (a) shows the force on the mirror for different voltages. The relative position of mirror and ESD is the position with the optimal force. (b) Shows how the force depends on the plate separation (assuming that the mirror is at the ideal operating position).

$$z_{\mathrm{dc}} = -F_{\mathrm{operating}} \cdot l/mg \approx 0.28\ \mu\mathrm{m}(\mathrm{at}1\ \mathrm{kV}). \tag{2}$$

From the equations (2) and (1) it also follows that the range is inversely proportional to mirror mass and plate separation. That is the reason why this new kind of ESDs is only suited for the case of small mirrors.

$$z_{\mathrm{dc}} \propto 1/(m \cdot d_{\mathrm{plates}}) \tag{3}$$

Figure 5(a) shows that the force that can be obtained scales quadratically with the applied voltage, when the mirror is in the operating position. This agrees very well with the prediction

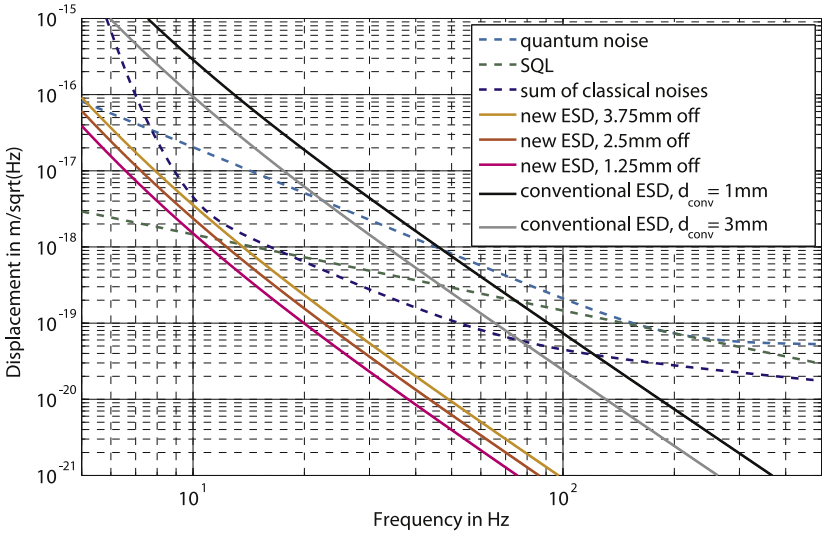

Figure 6. Comparison of seismic noise coupling in the AEI-10 m prototype interferometer for ESDs with the conventional design and our novel ESD configuration. The reddish traces indicate projections of how much table movement would couple into the interferometer if the novel ESD configuration is used, but the plates are not located ideally. The dashed lines indicate the sum of all classical noise (for example laser-, thermal-, seismic noise etc), quantum noise and the standard quantum limit (SQL) of the planned AEI-10 m sub-SQL interferometer. We have also included a projection of the seismic noise coupling if conventional ESDs mounted on the tables would be used, where d_{conv} indicates the distance between the mirror and the ESDs (grayish traces). As one can see, the seismic noise coupling of our novel ESD design is lower by about a factor 100 compared to a conventional ESD design.

from equation (1). The amount of force per voltage can be used to further characterize the ESD. If we write the quadratic relation as $F = \alpha U_{\mathrm{ESD}}^2$, then we obtain $\alpha = 1.4 \times 10^{-12}\,\mathrm{N\,V^{-2}}$. For comparison, the conventional ESDs in aLIGO and GEO 600 can deliver 2.9×10^{-10} and $4.9 \times 10^{-10}\,\mathrm{N\,V^{-2}}$, respectively ([13, 14]).

Figure 5(b) shows how the force changes when the plate separation is varied. The simple analytic model predicts an inverse square law (note that $\epsilon_{r_{\mathrm{eff}}}$ depends on the plate separation, as explained above), the FE model however returns a force inversely proportional to the fourth power of the plate separation. The stronger drop-off may be due a decreased region with homogeneous electrical field for large plate separations.

It is important to point out that the AEI-10 m prototype will have a hierarchical system of several actuators, of which the ESDs will be the ones with the smallest range and the fastest actuation. Coil magnet actuators with larger range will be located at the upper pendulum stages and in the seismically isolated tables. These actuators are however less suited for fast actuation, because above the pendulum resonances in the order of 1 Hz, the mirror movement will be filtered by the pendulum transfer function of f^{-2} per pendulum stage. The exact frequency range and expected rms actuation voltage of the ESDs will depend on the properties the aforementioned other actuators (not all of which are installed at the time of writing), as well as on the specific implementation of the longitudinal length control scheme.

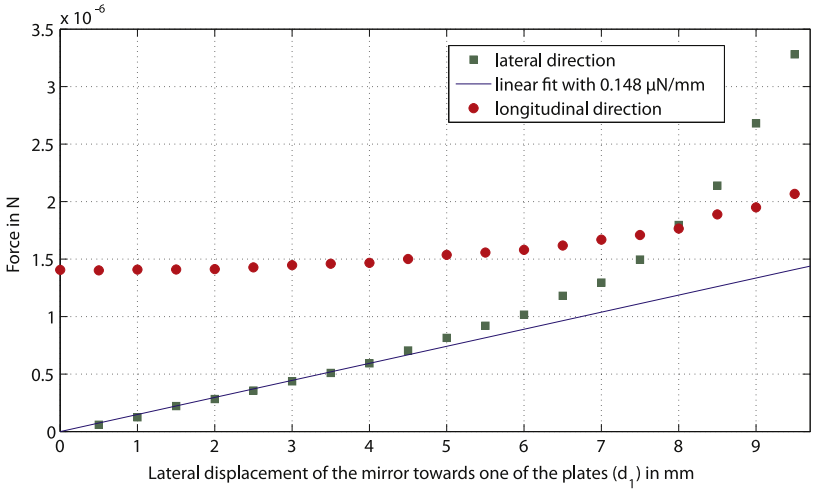

Figure 7. Lateral force on the mirror, versus relative lateral position of mirror and ESD.

4. Requirements and noise

Provided that the mirror and ESD are positioned correctly, the derivative of the force provided by the new ESD configuration, is zero. Together with the performance of the seismically isolated tables in the AEI-10 m prototype interferometer [12], it is possible to mount the new ESD directly to the table without additional seismic isolation. Figure 6 shows the expected coupling of seismic noise through the new ESDs for non-ideal positioning of the mirror in respect to the ESD plates. Even with the ESDs 3.75 mm off from the ideal longitudinal position, the noise contribution in the AEI-10 m interferometer would still be lower than the sum of all other classical noise sources at all frequencies.

In order to allow a direct comparison of the seismic coupling of a conventional ESD design and our new ESD design, we included the expected noise coupling from a conventional ESD design in figure 6 (see gray traces). For this analysis we assumed the force on the mirror for a conventional ESD design, which is given by [18]:

$$F = a \cdot \epsilon \cdot \epsilon_r \cdot U_{\mathrm{ESD}}^2 \cdot d_{\mathrm{conv}}^{1.5}, \tag{4}$$

where d_{conv} is the separation between the mirror and the ESD and a is a geometry factor that depends on the actual shape of the electrode pattern, and the dimensions of the mirror and the ESD. The strong scaling of the force with d_{conv}, explains the large coupling of seismic from the ESD to the test mass. For this analysis we assumed that both kinds of actuator provide the same longitudinal range and are bolted to the tables. The new ESD design provides a reduction in seismic noise coupling of about a factor of 100 compared to the conventional design.

Moreover, we also investigated how precisely the ESD plates (of the new design) have to be positioned in the direction along their surface normal. If the mirror is closer to one of the ESD plates, it will see a force towards the closer plate. This situation has been simulated using the FE model. The results can be seen in figure 7. If we arbitrarily set a limit for the force towards the closer plate to $1/10$ of the force in beam direction, then the mirror must be centered between the plates within less than 1 mm. For the case of small lateral displacements in the range of a few millimeters we can approximate the force in lateral direction to scale linearly with the lateral displacement. In this case the linear scaling factor is 0.148 $\mu\mathrm{N\,mm^{-1}}$.

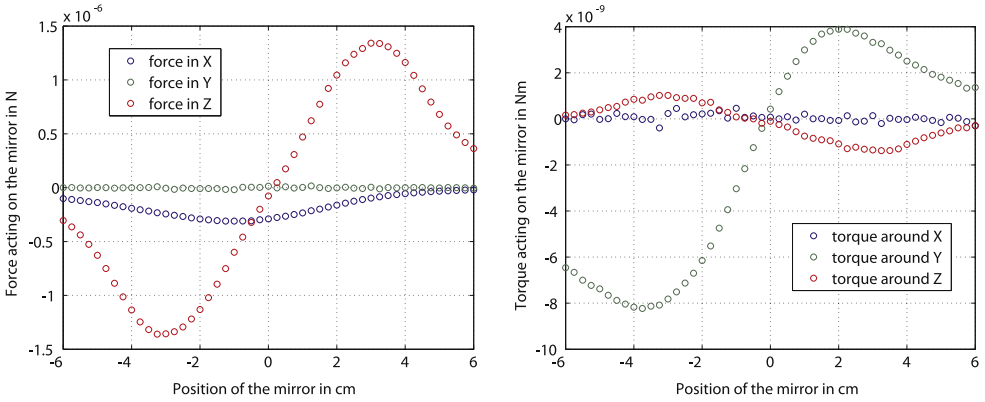

(a) Force (b) Torque

Figure 8. Force and torque with catcher. The catcher's position was kept constant (with the z-coordinate of its center of mass at -3.075 cm), while the mirror was moved.

All investigations in this work assume an uncharged mirror. Charges could be introduced to the mirror in several ways, for example by touching it, if the mirror touches the ESD plates, or through friction or migration of charges that may occur when evacuating or venting the vacuum system in which it sits.

We expect a significant change in the force provided by any kind of ESD for a charged mirror, and this is true for both the conventional type of ESD and for the presented geometry. It has been demonstrated in the past that UV light can be employed to reduce the total charge on the mirror [15]. However, the amount and distribution of charges that can be expected are not known, and will have to be determined experimentally.

5. The effect of asymmetries in materials in the vicinity of the ESDs

As mentioned earlier, the main optics of the AEI-10 m interferometer will be hung as a multi-stage pendulum, which is usually the case for gravitational wave detectors and their related, scaled-down prototyping facilities. In order to keep the mechanical losses low, the pendulum wires are typically dimensioned such that they are loaded to a significant amount of their breaking stress [16]. In the case of the AEI-10 m prototype, it is planned to use fused silica fibers with a diameter of 20 μm for the lowest pendulum stage. To protect the main optics if a fiber breaks, a 'catcher' will be placed underneath each suspended mirror. One could argue that such catchers may alter the performance of the ESDs proposed in this article, as they break the symmetry of the electrostatic environment close to the ESDs. Such asymmetries may introduce a (position-dependent) torque on the mirror, which would lead to coupling of longitudinal mirror motion to mirror alignment. We do not expect the same effect from symmetrically positioned parts around the ESDs. The goal of this section is to estimate upper limits due to this.

We simulated the effect of a sample configuration with catcher, which is modeled as a simple cuboid. In this simulation the ESD plates are at the sides of the mirror, similar in the mock-up drawing in the bottom right of figure 3. We use the same coordinate system as indicated in this image (but note that the actual FE model uses simple geometric shapes for the ESDs as in the top right of figure 3).

The catcher is positioned in such a way that it is centered below the mirror at the ideal operating point. It sits 1 cm below the mirror and is 4 cm tall. In the beam direction, the mirror projects from the ESD by 1 cm on each side. The catcher is 6.5 cm wide and is assumed to be at ground potential, while the ESD plates were set to $+500$ and -500 V. The results of the simulation are presented in figure 8.

Also there will be a torque around the *Y*-axis. Fortunately, the torque around the *Y*-direction, which is the strongest, is flat to first order when the catcher is centered with respect to the mirror. It is important to note that this crude catcher geometry is used as a worst case scenario to set an upper limit. Still, this analysis showed that a metal catcher, as it is usually used, can introduce a coupling of longitudinal actuation to other degrees of freedom. This should be kept in mind when designing mechanical structures such as the catcher in close vicinity of the ESDs. To reduce the influence of mechanics around the mirror, one may, for example, use a different catcher geometry or material, such as Macor or polyether ether ketone, a vacuum compatible polymer. Another way may be to increase the distance between catcher and the mirror. The AEI-10 m interferometer suspension will feature 'fiber guards', an aluminium semi-enclosure around the fibers that suspend the mirror. Their presence will necessitate the ESDs to be installed at the top and bottom of the mirrors. A detailed description of the design of the AEI-10 m prototype suspensions can be found in [17].

6. Details and verification of the FE model

As the work presented in this article relies heavily on the use of FEM simulations, it is crucial to validate them.

A good method of validating the results obtained by the FE model is to compare it to an analytic model. In the case of this work, a simplified analytic model has been presented in section 2, with the result that the force obtained via the analytic model is in the same order of magnitude as predicted by the FE model.

Another important aspect of any FE model that needs to be evaluated is its meshing. In this work, we used a mesh of three-dimensional hexahedral elements (SOLID122) for the ESD plates and the mirror, as can be seen in figure 3. The space around them was modeled using the same type of elements in tetrahedral shape.

The mesh size, i.e. the size of the FEs, is a trade-off in most kinds of FE analysis. A finer mesh will yield more accurate results at the expense of time needed for the computation. To find a good compromise for the mesh size for this work, we performed a mesh convergence analysis. In this analysis we computed the force on the test mass in the FE model at the ideal operating point, and we repeat this computation for different mesh sizes. For this, we introduce a parameter M_{div}, which defines the number of FEs along linear edges of the model, for example the long edges of the ESD plates. Furthermore, to reduce computational cost, we define that the ESD plates should have $M_{\mathrm{div}}/4$ elements in height. This is justified by the geometry of the plates, and that as conductor, the electric field in them should be small.

Figure 9 shows the result of the mesh convergence analysis. As expected, the resulting force changes with the mesh size with stronger change for a more coarse meshing than for a finer one. Based on figure 9, we picked a mesh density of 15 elements per line for the analysis presented in this work. Assuming that the finest mesh with 28 elements per line is accurate, we can estimate the error introduced by picking the more coarse mesh with 15 elements per line by comparing the force at both mesh densities. It differs by about 3%, which we will assume is the accuracy of the presented analysis.

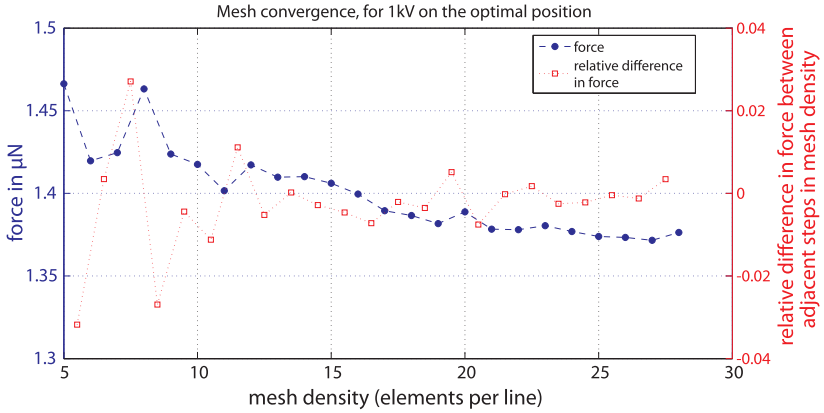

Figure 9. This plot shows the resulting force on the mirror in the investigated scenario in dependence of the mesh size.

7. Summary and outlook

We presented a novel type of ESD for longitudinal test mass actuation in prototypes and table top interferometers in the field of gravitational wave detectors. The ESDs would be plates installed at the sides of the test masses. For the AEI-10 m prototype, this type of ESD could be mounted directly to the seismically isolated table. We find that the ESDs would have to be positioned with an accuracy of better than 3.75 mm longitudinally and 1 mm in lateral direction. They could move the mirror by more than 0.28 μm with 1 kV and by more than 1 μm when operated at 2 kV. One aspect that has not been investigated so far refers to the noise terms originating from electrical charges on the test masses. While it would be straightforward to include these in our FE analysis, it is not clear at all what amount of charge and geometrical charge distribution would be sensible to assume. Therefore this aspect needs to be tested experimentally. This work is now underway.

Acknowledgments

We thank P Fritschel for useful comments on the manuscript. The authors would like to acknowledge the support from the Max Planck Society, the European Research Council (ERC-2012-StG: 307245) and the Science and Technology Facilities Council (STFC, ST/L000946/1). This work was performed as part of our International Max Planck Partnership (IMPP) with the Max Planck Society, supported by SFC, EPSRC and STFC.

References

[1] Affeldt C *et al* 2014 Advanced techniques, in GEO 600 *Class. Quantum Grav.* **31** 224002
[2] Harry G M (For the LIGO Scientific Collaboration) 2010 Advanced LIGO: the next generation of gravitational wave detectors *Class. Quantum Grav.* **27** 084006
[3] Degallaix J *et al* 2013 Advanced Virgo Status, *9th Symp. Proc. Conf.* (*Bibliothque Nationale de France, Paris, 21–25 May 2012* (*ASP Conference Series* vol 467) (San Francisco: Astronomical Society of the Pacific) p 151
[4] Aso Y *et al* 2013 Interferometer design of the KAGRA gravitational wave detector *Phys. Rev.* D **88** 043007

[5] Aston S M *et al* 2012 Update on quadruple suspension design for Advanced LIGO *Class. Quantum Grav.* **29** 235004
[6] Dolesi R *et al* 2011 Brownian force noise from molecular collisions and the sensitivity of advanced gravitational wave observatories *Phys. Rev.* D **84.6** 063007
[7] Gräf C *et al* 2012 Optical layout for a 10 m Fabry–Perot Michelson interferometer with tunable stability *Class. Quantum Grav.* **29** 075003
[8] Gossler S *et al* 2010 The AEI 10 m prototype interferometer *Class. Quantum Grav.* **27** 084023
[9] www.speed-meter.eu
[10] Graef C *et al* 2014 Design of a speed meter interferometer proof-of-principle experiment *Class. Quantum Grav.* **31** 215009
[11] Margulies S 1984 Force on a dielectric slab inserted into a parallel-plate capacitor *Am. J. Phys.* **52** 515–8
[12] Wanner A *et al* 2012 Seismic attenuation system for the AEI 10 m prototype *Class. Quantum Grav.* **29** 245007
[13] Shapiro B, Brett H, Mavalvala N and Youcef-Toumi K 2011 Actuator sizing of a quadruple pendulum for advanced gravitational wave detectors, *American Control Conf.* (*ACC*) (Piscataway, NJ: IEEE)
[14] Strain K A 2006 Electrostatic drive (ESD) results from GEO and application in advanced LIGO technical note T060015-00-K (https://dcc.ligo.org/LIGO-T060015/public)
[15] Hewittson M *et al* 2007 Charge measurement and mitigation for the main test masses of the GEO 600 gravitational wave observatory *Class. Quantum Grav.* **24** 6379
[16] Tokmakov K V 2012 A study of the fracture mechanisms in pristine silica fibres utilising high speed imaging techniques *J. Non-Cryst. Solids* **358** 1699–709
[17] Hammond G paper in preparation
[18] Grote H 2003 Making it work: second generation interferometry in GEO 600! *PhD Thesis* University of Hannover
[19] ANSYS Inc. Southpointe 2600 ANSYS Drive Canonsburg PA 15317 USA (www.ansys.com)